Chapter 5
Farallon Subduction Affecting North American Tectonics[4]

5.1 The Enigmatic Laramide Orogeny

With an inverse convection model, we recovered the Farallon plate subduction from its present-day mantle remnants, and we predicted the Western Interior Seaway (WIS) formation as due to dynamic subsidence associated with broad shallow to flat down-going slabs underneath North America during the Late Cretaceous (Chapter 4). Now we will move on to investigating another enigmatic tectonic feature, the Laramide orogeny.

The Laramide orogeny is an orogenic event occurring in the Late Cretaceous to Paleocene (80–55Ma), during which widespread thick-skinned Laramide block uplifts and the Rocky Mountain fold-and-thrust belt formed in the United States, which, in a broader

---

[4] This chapter is based on: 1) Liu, L., M. Gurnis, M. Seton, J. Saleeby, R.D. Müller & J. Jackson (2010), *The role of oceanic plateau subduction in the Laramide Orogeny,* Nature Geoscience, doi: 10.1038/NGEO829. ***Author contribution:*** L.L. and M.G. designed the whole workflow and carried out the inverse convection model, M.S. and R.D.M. carried out the plate reconstruction, J.S. worked on the geological interpretation and J.M.J. provided mineral physics analysis. All authors participated in preparing the paper. 2) Liu, L. and M. Gurnis (2010), *Dynamic subsidence and uplift of the Colorado Plateau,* Geology, doi:10.1130/G30624.1, in press. 3) Liu, S., D. Nummedal and L. Liu, *Tracking the Farallon plate migration through the Late Cretaceous Western U.S. Interior Basins,* Geology, in review. ***Author contribution:*** S.L. and D.N. backstripped the stratigraphy in WIS basins, L.L. provide the inverse convection model. All authors participate in writing the paper. 4) Spasojevic, S., L. Liu, M. Gurnis & R.D. Muller (2008), *The case for dynamic subsidence of the United States east coast over the Cenozoic*, Geophys. Res. Lett., 35, L08305, doi:10.1029/2008GL033511. ***Author contribution:*** S.S. analyzed the paleo-shoreline migration and sea level curves; L.L. performed the inverse convection model; M.G. supervised the whole workflow.

definition also includes the formation of the Canadian Rocky Mountains and the Sierra Madre Oriental fold-and-thrust belt in Mexico [English and Johnston, 2004, Fig. 30]. Compared to the North American Cordillera system, which sustained through the Jurassic and Early Cretaceous and represents thin-skinned deformations, the Laramide events are much more restricted in time and involve deformation of the entire basement over the western U.S. The extent of Laramide structures reaches a maximum 1500 km inboard (Fig. 30), much farther inland than a typical mountain belt along convergent plate boundaries [e.g., Saleeby, 2003]. Furthermore, the basement-involved deformations largely form a narrow "corridor" from Southern California toward Colorado and Wyoming [Saleeby, 2003].

Mechanisms for the Laramide Orogeny have been debated for decades, with little consensus reached at present [Burchfiel *et al*., 1992; DeCelles, 2004; English and Johnston 2004]. At least four different conceptual models have been proposed (Fig. 31). The "Retroarc Thrusting" mechanism proposed by Price [1981] attributed the inboard Laramide deformations to back-thrusting of the Cordillera onto the adjacent continental interior due to strong regional compressive stresses (Fig. 31A). An "Orogenic Float" tectonic model assumes a major through-going deep crustal basal detachment, which allows collision at plate boundary to be transmitted far inland (Fig. 31B). The "flat slab subduction" model argues that basal traction from the flat lying slab caused the basement-cored uplifts (Fig. 31C). A final model called "Cordilleran Transpressional Collision" assumes that much of

the Canadian Cordillera travelled thousands of km northwards, and this translation caused compressions over the western part of North America (Fig. 31D).

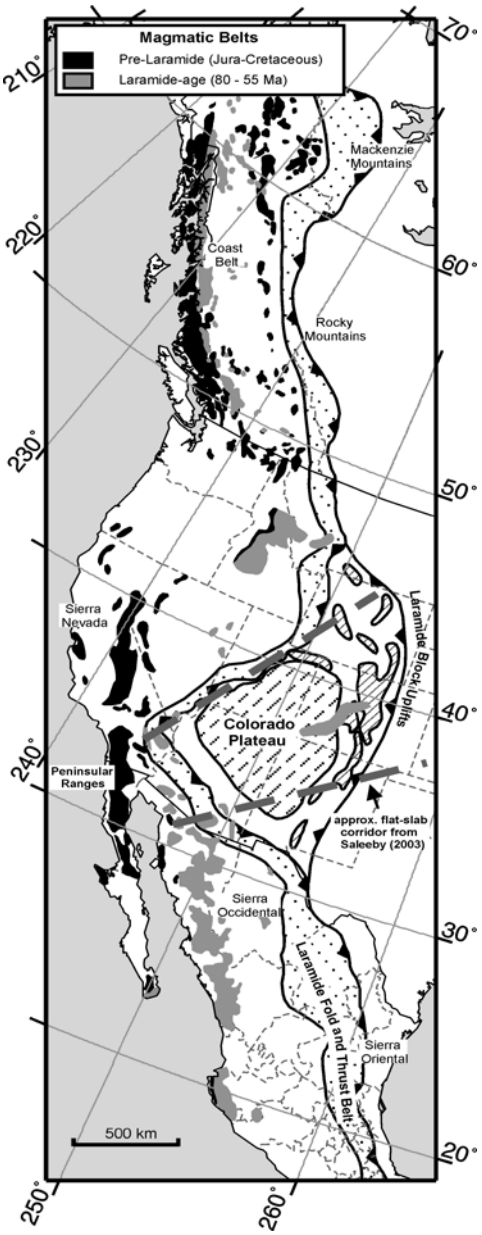

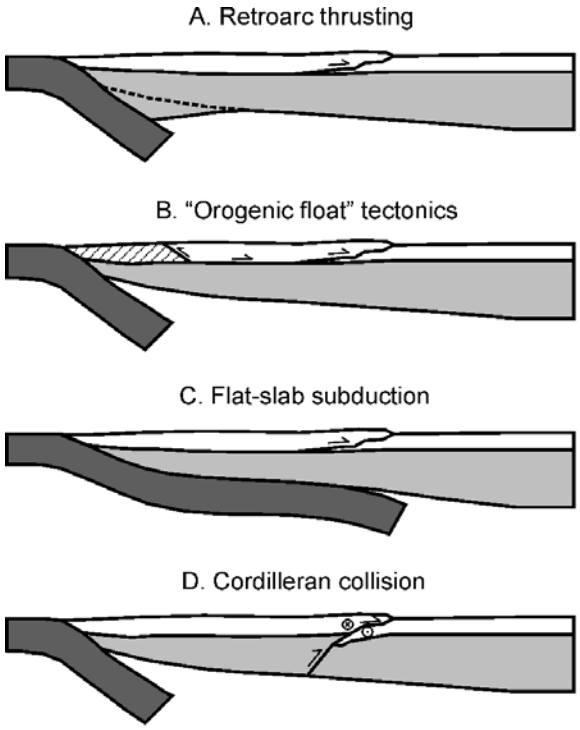

Figure 31 (From English and Johnston, 2004) A sketch diagram showing the various models proposed to explain the inboard deformation belt of the Laramide orogeny.

Figure 30 (From English and Johnston, 2004) Maps of pre-Laramide and Laramide magmatism, the extent of the Laramide thin-skinned fold-and-thrust belt and thick-skinned block uplifts, and the approximate location of the Laramide flat slab, according to Saleeby (2003).

A viable way to test a model is to check whether it can satisfactorily explain most features associated with the Laramide Orogeny. Among these conceptual models (Fig. 31), the flat slab subduction mechanism caused by subduction of either the Farallon-Kula ridge

[Henderson *et al.*, 1984] or a buoyant oceanic plateau [Livaccari *et al.*, 1981; Saleeby, 2003], seems the most promising [English and Johnston, 2004]. However, independent verification of these subduction models has remained elusive, because the putative ridge or plateaus are no longer on the surface. Previously, the plateau subduction model has been investigated through the reconstruction of synthetic conjugates to the plateaus in the western Pacific today [Livaccari *et al.*, 1981; Tarduno *et al.*, 1985], but these models differ substantially from each other depending on the underlying plate kinematic models, and the role of plateau subduction in driving Laramide deformation remains unclear.

The inverse model of mantle convection based on seismic tomography we have developed allows reconstruction of the history of subduction, providing a link between present-day mantle structures and geological observations (Chapter 4). This approach has the potential of recovering the now subducted former oceanic plateaus back to the surface directly from the observed present-day mantle seismic structures. Furthermore, since the plate motions involved in the calculation extend back to the time of interest, the larger uncertainties from earlier stages are avoided. The inverse calculation, therefore, offers a complementary approach to inferring the position of the oceanic plateau back in time. Here, we combine both forward (kinematic) and inverse (dynamic) approaches with geological observations from the overriding plate to test the hypothesis of plateau subduction.

5.2 The Role of Oceanic Plateau Subduction in the Laramide Orogeny

5.2.1 Detection of Oceanic Plateaus with Plate Reconstruction

We first use a recent plate reconstruction model to predict the positions of oceanic plateaus subducting beneath North America during the Late Cretaceous. The predicted positions of the Shatsky and Hess conjugates on the Farallon plate during the Late Cretaceous are shown in Fig. 32. The reconstructed Shatsky conjugate intersects the North American continent at ~90 Ma in southern California, and the Hess conjugate intersects the northern part of Mexico at ~70 Ma (Fig. 32A).

In the reconstruction, we assume that the Shatsky Rise formed at the Pacific-Farallon-Izanagi triple junction [Sager *et al*., 1988; Nakanishi *et al*., 1999] between ~145–130 Ma with conjugates on the Farallon and Izanagi plates. The Hess Rise and its conjugate formed along the Pacific-Farallon ridge at ~110 Ma. An ellipsoidal configuration is assumed for these conjectured plateaus, with contours representing estimated maxima and minima extent of the now subducted plateau conjugates. Positions of the conjugate plateaus are inferred based on the geometry of the preserved plateaus, the age of the underlying ocean lithosphere and the associated mid-ocean ridge system. The Pacific-Farallon ridge was reconstructed by deriving stage rotations from half-stage rotations with an assumption of spreading symmetry [Muller *et al*., 2008]. Reconstruction of the Pacific-Izanagi-Farallon triple junction additionally followed principles of triple junction closure [McKenzie and Morgan, 1969]. The absolute reference frame used for the Pacific plate is based on a hybrid moving Indian-Atlantic hot-spot [O'Neill *et al*.,

2005] and a fixed Pacific hotspot reference frame for times prior to 83.5 Ma [Wessel *et al*., 2006]. Although motion between hotspots in the Indian-Atlantic and Pacific domains has been recognized [Molnar & Atwater, 1973; Tarduno *et al*., 2003; Tarduno *et al*., 2009], moving Pacific hotspots have not been incorporated into our model as there are no published rotations available. Instead, we test two alternative fixed Pacific hotspot reference frames for times prior to 83.5 Ma [Wessel *et al*., 2006; Wessel & Kroenke, 2008] and find a difference of < 300 km between models at 90 Ma. We do not anticipate significantly more than 300 km of motion using a moving hotspot reference model over this 6.5 million year period (from 83.5–90 Ma) as this would require higher rates of motion of the Pacific plate for which there is no evidence.

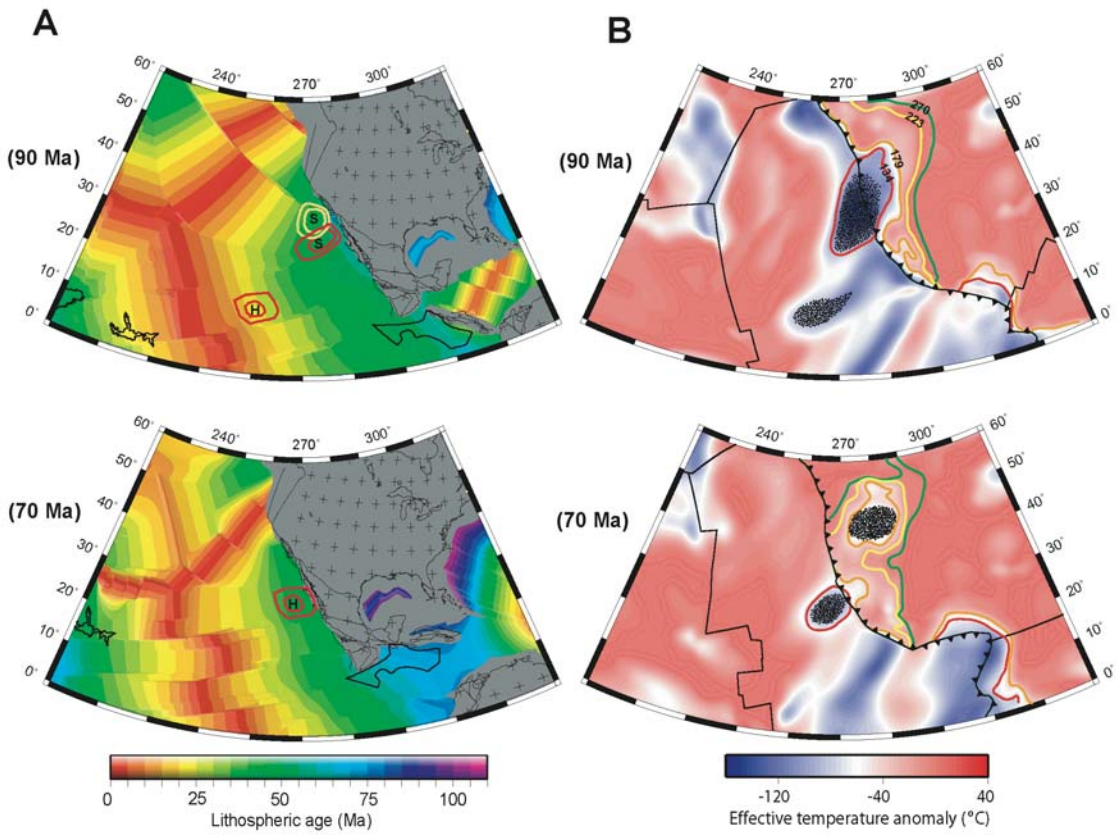

Figure 32 Predicted positions of the Shatsky and Hess conjugates in Late Cretaceous from (A) plate reconstruction and (B) inverse convection models. A. The Hess (H) and Shatsky (S) conjugate plateaus forming along the Pacific-Farallon (Farallon-Izanagi) ridges are denoted by red (yellow) contours; the contours represent their maximum/minimum extents while overlying the age of the sea floor [Muller *et al*., 2008]. Black outlines denote major presently preserved oceanic plateaus. B. Tracers delineate locations of the thickest part of the recovered lithosphere above 179 km depth from inverse convection models starting with seismic tomography, where the background effective temperature is color coded. Color contours show isotherms at different depths (labels in km) of effective temperature anomalies 40 °C lower than ambient mantle.

On the other hand, we perform an inverse calculation of mantle convection starting with a shear wave seismic tomography model [Grand, 2002]. The model that best fits stratigraphy over the western U.S. reveals an epoch of flat slab subduction characterized by a thicker-than-ambient oceanic lithosphere on the Farallon plate during the Late Cretaceous [Liu *et al*., 2008]. We highlight the thickest part of this segment of lithosphere with passive tracers in order to illustrate its location, and run the model forward from 100 Ma to the present. At 90 Ma, the thickened lithosphere is located largely to the west of the Farallon subduction zone while its northeast flank is subducted beneath North America initiating a segment of shallow flat subduction (Fig. 32B). The thickened lithosphere denoted by tracers falls in almost the same area as the kinematically predicted Shatsky conjugate, with both its orientation and geometry in the two models reasonably correlative (Fig. 32). At 70 Ma, the entire area of this thickened lithosphere shifts below the western U.S., while a second flat slab segment forms to the south correlative with the predicted position of the Hess conjugate (Fig. 32A,B).

Since the plate reconstruction approach starts with positions of the extant Shatsky and Hess plateaus while the inverse convection approach utilizes the seismic structures of the present-day mantle, the two approaches are independent, although they share the same plate reconstruction from 90 Ma to the present. Both temporal and spatial consistencies of these now subducted plateaus from the two approaches suggest that these features existed on the Farallon plate during the Cretaceous. Identification of these oceanic plateaus allows a quantitative assessment of their relation to the sequence of geological events over western U.S., especially those of the Laramide Orogeny.

5.2.2 Mechanisms for the Laramide Orogney

Traditionally, plateau subduction is thought to cause synchronous crustal uplift. Therefore, earlier models attributed the Laramide Orogeny to subduction of conjugates of either the Hess [Livaccari *et al.*, 1981] or Shatsky Rise [Tarduno *et al.*, 1985] between roughly 70–60 Ma, the time of classic Laramide exhumation [DeCelles, 2004]. However, we find that this relationship is only true along the continental margin where the plateaus initially entered the subduction zone. Initial subduction of the Shatsky conjugate beneath southern California in both up-to-date plate reconstructions and inverse convection models (Fig. 32) correspond to fore-arc destruction, intra-arc ductile thrusting and rapid exhumation of the southern Sierra Nevada batholith (SNB) during 96-86 Ma[12] (Fig. 26, Fig. 33). Continuing subduction of the Shatsky conjugate progressively disrupted the southern California active margin producing the distinctive southern California batholith (SCB) segment (Fig. 33), characterized by severe tectonic erosion of the fore-arc and

frontal arc, shearing off of the mantle wedge and lower crust, and shallow-level underplating of trench sediments [Saleeby, 2003; Ducea *et al.*, 2009]. Crustal structure of the SCB is currently dominated by the effects of large magnitude Late Cretaceous extension that followed immediately the passage of Shatsky conjugate [Saleeby, 2003], marked in Figure 33 by the much broader SCB than the SNB and the Peninsular Ranges batholith (PRB).

Proximal to the SCB segment both the SNB and PRB segments experienced Late Cretaceous intra-arc ductile thrusting, and parallel forearc unconformities, presumably in response to the subduction of the flanks of the Shatsky conjugate [George and Dokka, 1994; Nadin and Saleeby, 2008]. Large volume magmatism of both the SNB and SCB ceased at ca. 85 Ma, while diffuse supra-subduction magmatism migrated hundreds of kilometers inland [Burchfiel *et al.*, 1992]. The PRB segment of the active margin responded to Hess conjugate subduction, commencing at ca. 65 Ma (Fig. 33), in a more subdued fashion than the SCB response to Shatsky conjugate subduction. The PRB underwent rapid erosional denudation as arc magmatism migrated abruptly inland to Sierra Madre Occidental [Ferrari *et al.*, 2007], and crustal shortening intensified along the Mexican foreland thrust belt, which is considered to be the southward continuation of the Laramide orogeny [Campa, 1985]. A plausible explanation for the differences in intensities of Shatsky and Hess conjugate damage zones is a notable difference in their masses (Fig. 32).

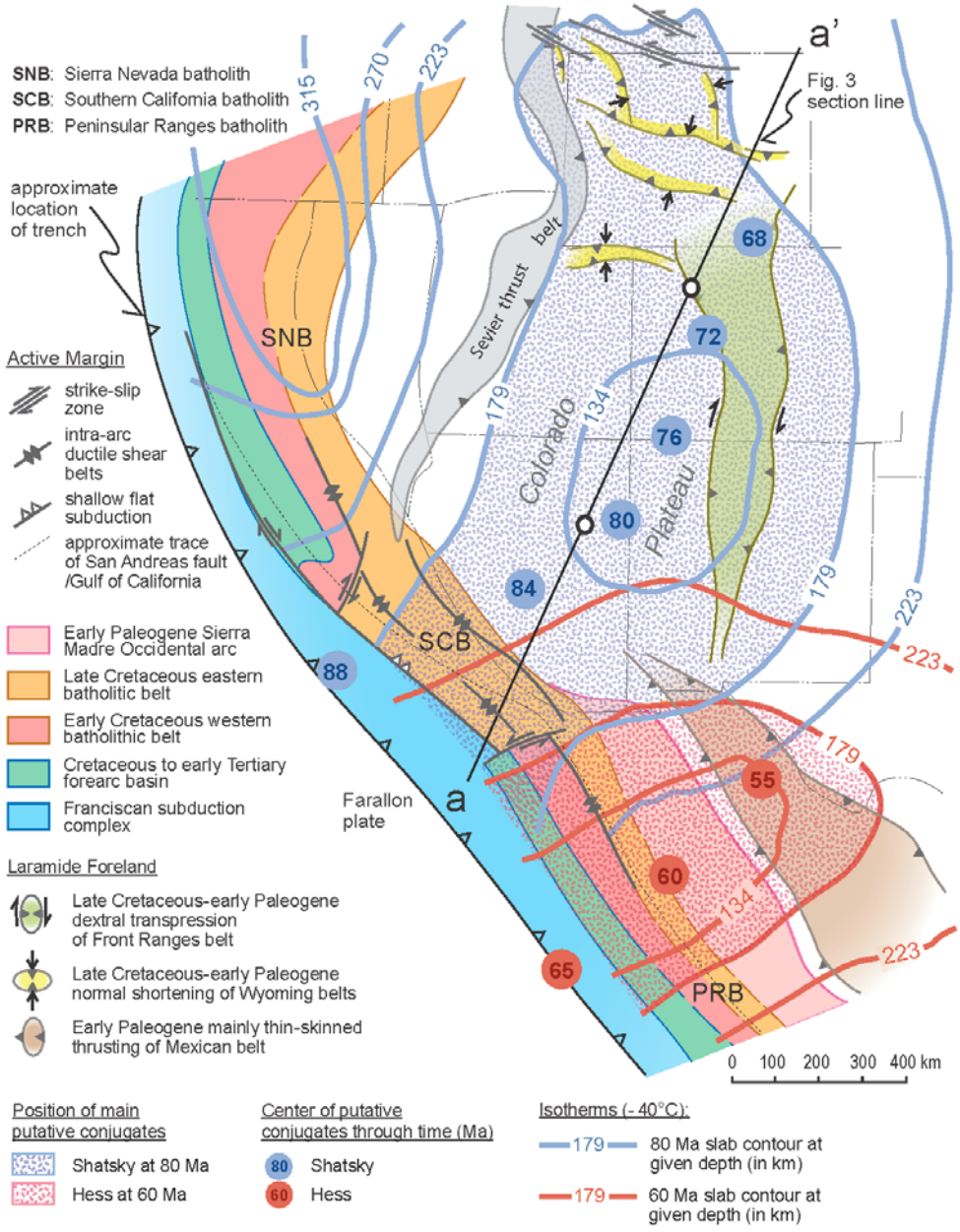

Figure 33 Palinspastic map showing SW Cordilleran active margin and Laramide foreland for end of Cretaceous time with temperature field overlain. Contours (same as Fig. 30; light blue for 80 Ma, red for 60 Ma) and predicted positions of the putative Shatsky and Hess conjugate plateaus (inside the 179 km contour) are from the inverse model. Filled circles represent the volumetric

center of the putative Shatsky (light blue) and Hess (red) conjugate plateaus at given age during their subduction beneath North America. Line a-a' indicates the surface trace of cross-sections shown in Figure 34.

Flat subduction of the Shatsky conjugate during the Late Cretaceous appears to have caused the shortening and faulting inside the classic Laramide province, which flanks the northern and eastern margins of the Colorado Plateau (CP) (Fig. 33). The classic Laramide is distinguished from the Jurassic-Cretaceous thin-skinned Sevier thrust belt by the intimate involvement of cratonic basement and a more restricted timing of Late Cretaceous–early Paleogene [Burchfiel *et al*., 1992]. Our reconstruction places the center of the Shatsky conjugate moving in a northeast arcuate path beneath the CP region between 84 and 68 Ma (Fig. 33). Both the NE trajectory and northward tapering of the plateau thickness correlate with Late Cretaceous–early Paleogene dextral transpression along the Front Ranges belt that transfers northwards into normal shortening across the Wyoming belts [Karlstrom and Daniel, 1993] and sinistral shear to the north [Burchfiel *et al*., 1992] (Fig. 33). While localization of deformation along the Front Ranges and northern Wyoming was facilitated by reactivation of ancient basement structures [Burchfiel *et al*., 1992], shortening in between seems mainly due to NE subcrustal thrusting of the Shatsky conjugate. Sevier belt deformation during the NE motion of Shatsky conjugate along its foreland entailed the final phases of thrusting [DeCelles, 2004] transitioning into the initiation of regional extensional tectonism [Druschke *et al*., 2009]. The migration of the western edge of the Shatsky conjugate along the Sevier belt

(Fig. 33) implies a distinct mechanism for classic Laramide deformation, relative to that of the Sevier belt.

In contrast to earlier plate reconstructions [Livaccari *et al.*, 1981; Tarduno *et al.*, 1985], our analysis predicts the continuation of Late Cretaceous marine conditions across much of the Laramide province. This is the time when the WIS occupied most of the western and central North America (Fig. 14), as is well documented in isopach maps distributed over the Colorado Plateau and areas to its north and east, called the Great Plains [e.g., Bond, 1976; DeCelles, 2004]. Even in regions to the south of the Colorado Plateau, where little Cretaceous marine sediment has been preserved probably due to erosion, a recent low temperature thermochronology study based on apatite (U-Th)/He inferred that the southern Plateau and surrounding area must have been buried by at least 1.5 km thick of sediment during the Late Cretaceous [Flowers *et al.*, 2008]. According to our study, such widespread marine sedimentation is due to long-wavelength dynamic subsidence associated with the flat slab underlying these areas (Fig. 34A, B). Collectively, our study suggests that initial subduction of the plateau should have caused the slab to flatten because of the extra buoyancy associated with its thick crust, but continuing flattening would mostly result from the increased plate coupling with a possibly weakened mantle wedge [Manea and Gurnis, 2007]. As the Shatsky conjugate translated beneath the Colorado Plateau region (Fig. 33), the oceanic crust is deep enough to undergo the basalt-eclogite phase transformation, during which the plateau loses its positive buoyancy [Ringwood and Green, 1966]. Both the overall negative slab density anomaly and enhanced plate coupling during shallow subduction drag the surface downward (Fig. 34A). This phase change is not

incorporated in the inverse model, and should be addressed in future research simulating the flattening process of a slab due to subduction of an oceanic plateau.

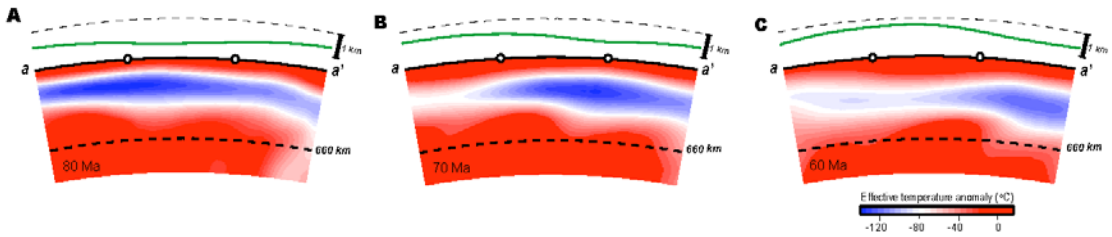

Figure 34 Configuration of the subducting Farallon flat slab and the corresponding surface dynamic topography along profile a-a' (shown in Fig. 33). Three representative times (A–C) during Late Cretaceous to Early Paleocene are chosen. The dynamic topography is shown with green lines.

A present-day analogy to this situation (e.g., shown in Fig. 34A) is the subducting Inca plateau in Peru [Guscher *et al.*, 1999], where broad surface subsidence is observed above the flat slab outlined by seismicity (Fig. 35). In a recent seismic tomography model [Li *et al.*, 2008], the putative Inca plateau shows up as a prominent P wave anomaly whose geometry and location correlate well with the flat portion of the subducting oceanic slab, and with a surface topography low. The similarity between the still subducting Inca plateau and the reconstructed Shatsky conjugate plateau further strengthens our argument that an oceanic plateau, once migrated inland, will cause surface subsidence instead of uplift.

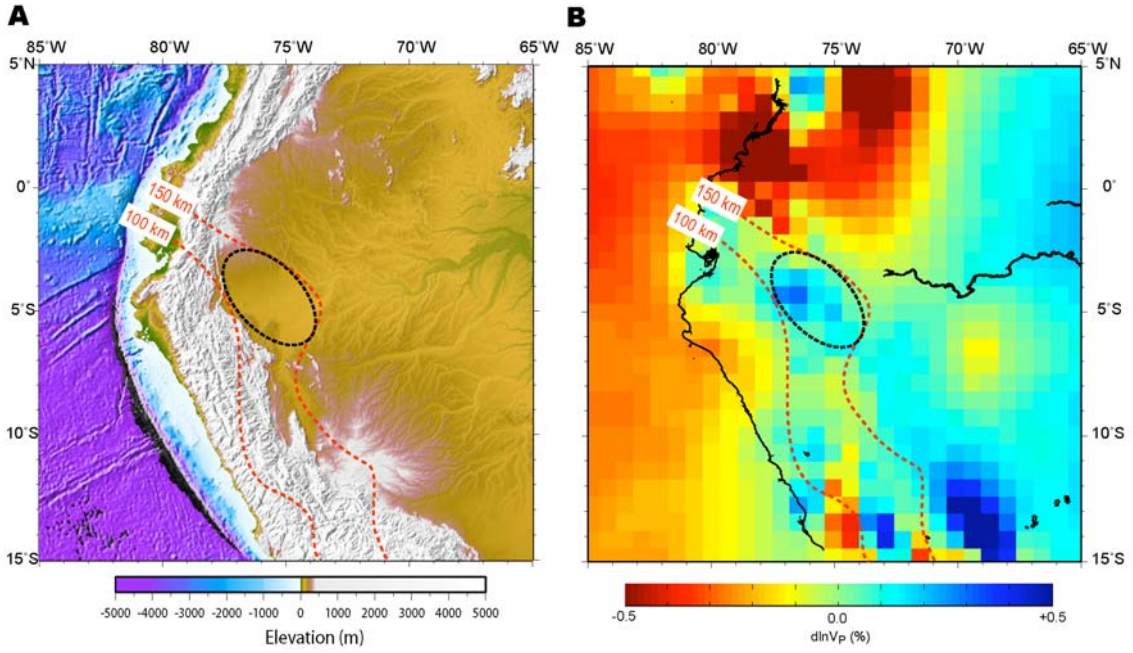

Figure 35 Surface topography (A) and seismic tomography [Li *et al.*, 2008] at 120 km depth (B) of western South America. The dashed red lines indicate slab contours [Guscher *et al.*, 1999] at 100 and 150 km depth, respectively. The dashed black ellipse represents the putative Inca plateau subducting beneath Peru [Guscher *et al.*, 1999]. Note the topography low (presumably subsidence) above the Inca plateau, which shows up as a fast seismic anomaly in B. Both surface subsidence and flat slab formation associated with the subducting Inca plateau makes it a present-day analogy of our model where subduction of the Shatsky conjugate plateau caused the slab to flatten while simultaneously inducing surface subsidence above the plateau during the Late Cretaceous.

Furthermore, our study suggests a mechanism for the Laramide uplift that is different from earlier thoughts. We find that Laramide uplifts at local scales should have initiated along thrust faults [DeCelles, 2004], when the flat slab underplated the Laramide province (Fig. 33). Although not modelled explicitly, this process should reflect relative topography/relief changes in response to crustal thickening and brittle failure subject to

strong basal traction and compression exerted by the plunging oceanic plateau. Subsequent regional scale uplifts, however, are associated with removal of the plateau from beneath the Laramide province. The flat slab associated with the Shatsky conjugate gradually sank deeper into the mantle as it migrated to the northeast. Both horizontal removal of flat slab from beneath the CP region after 80 Ma and the overall diminishing negative dynamic topography associated with cold slabs (Fig. 34B, C) led the surface to rebound in a SW to NE trend with a maximum of ~600 meters uplift occurring during the Latest Cretaceous over the CP (Fig. 34). This corresponds to regional uplifts starting as early as 80 Ma and peaking at 70–60 Ma across the Laramide province, and the overall eastward migration of marine conditions from the Sevier foredeep region to regions further into the continental interior [DeCelles, 2004].

The exact history and amounts of the uplift has been another widely debated issue. Our model predicts that the Laramide province experienced two stages of uplift, with an accumulative uplift by Eocene of about 1.2 km, consistent with the inferred kilometer-scale rock uplift over the southern CP [Flowers *et al*., 2008]. In Section 5.3, I will discuss the uplift history over the Colorado Plateau region in more detail. Removal of the Shatsky conjugate by its sinking north-eastward into the mantle may have further facilitated fault reactivation causing distributed basement uplifts intervened by the Laramide foredeep basins [Burchfiel *et al*., 1992; DeCelles, 2004], although we do not yet understand the details of the process. Our study may explain the 20 Myr time lag between the Late Cretaceous (~80 Ma) shortening deformations and Early Paleocene (~60 Ma) cooling events of the Laramide Orogeny [DeCelles, 2004].

5.2.3 Present-day Position of the Subducted Plateaus

Can a subducting oceanic plate always penetrate into the lower mantle, and where does the crustal material end up after subduction? It is generally accepted now that whole-mantle convection dominates although some slabs still get stagnated at the upper-lower mantle interface [Fukao *et al.*, 1992; Li *et al.*, 2008]. Mineral physics calculation suggests that the crustal material should also get subducted into the lower mantle accompanying the downgoing oceanic slab [Hirose *et al.*, 1999]. Direct image of lower mantle remnant crusts, however, has not been obtained, leaving many aspects of their elastic and dynamic properties unknown. Therefore, locating and verifying the existence of the foundered oceanic plateaus (with thick crusts) inside the present-day mantle will be of significance to several fields of earth sciences, including seismology, geodynamics, and mineral physics.

If our arguments about oceanic plateau subduction are reasonable, the geodynamic model we construct can predict the locations and geometries of the deeply subducted plateau conjugates in the present-day mantle via tracers (Fig. 36). By tracing the two oceanic plateaus to the present day, we find that both conjugates are now situated under the east coast of the U.S., with the Shatsky conjugate to the east of the Great Lakes and the Hess conjugate to the south. The Shatsky conjugate is predicted to extend from 900 to 1400 km in depth, covering ~1000 km in the north-south direction and ~500 km east-west; the Hess conjugate essentially stays above 1000 km depth with ~500 km cross-sectional dimensions (Fig. 36). In a recent high-resolution P wave seismic inversion [Li *et al.*, 2008], very similar configurations of the Farallon remnant structures are observed, compared to those in the S wave tomography (Fig. 13), reinforcing the interpreted

positions of these oceanic plateau conjugates. We emphasize that the tracers outlines the possible location ranges of these sank plateaus, and the smearing effect of global tomography inversions tend to blur/average the signature of these plateaus during the seismic imaging process.

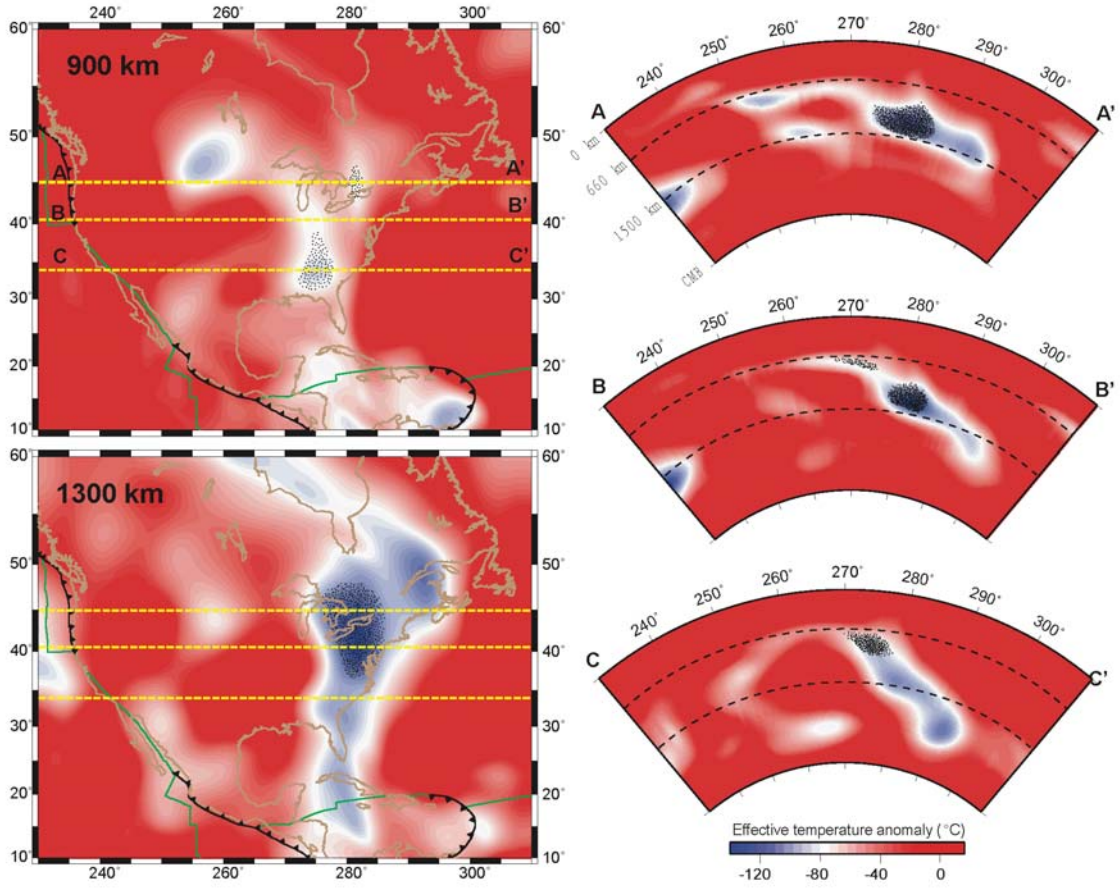

Figure 36 Location and geometry of the Shatsky and Hess conjugate plateaus inside present-day mantle. Map view at two different depths (900 and 1300 km) and cross-sectional view at three latitudes (45°, 41° and 33° North) are shown. Tracers highlight the predicted locations and distributions of these plateaus. The Shatsky conjugate is to the east of the Great Lakes and the Hess conjugate is to the south.

Stishovite-structured silica, one of the main proposed constituents of deeply subducted mid-ocean-ridge basalt (MORB) [Hirose *et al*., 1999], has seismic velocities ~20% higher than the ambient mantle after the post-stishovite phase transition (P_{tr}) [Carpenter *et al*., 2000]. In MORB, incorporation of a few wt. % Al_2O_3 and H_2O into silica is favorable [Hirose *et al*., 1999; Lakshtanov *et al*., 2007] and decreases the depth of post-stishovite P_{tr} to ~800 km [Lakshtanov *et al*., 2007]. Although effects of temperature on the wave speeds of post-stishovite are unknown, an estimated decrease by <4% in the lower mantle is reasonable [Cammarano *et al*., 2003]. Therefore, ~25% of hydrous aluminous post-stishovite in deep MORB crust would cause seismic velocity anomalies >4%, where current tomography models are blurry. Because of the substantially thicker-than-ambient crust accreted during formation of an oceanic plateau and expected slab thickening upon entrance into the lower mantle, present remnants of the Shatsky and Hess conjugates could have an accumulated crustal pile thickness of >50 km. The predicted strong seismic anomalies in conjunction with the large volumes should make these foundered crustal blocks detectable as sharp seismic features, in which travel time anomalies and waveform multi-pathing are expected [Sun *et al*., 2009]. The ongoing seismic experiment with the USArray shifting to the east coast of U.S. should provide the opportunity to detect these subducted oceanic plateau conjugates.

5.3 Dynamic Subsidence and Uplift of the Colorado Plateau

5.3.1 Background

The Colorado Plateau is a distinct geologic province in the southwestern United States bounded by the Basin and Range province to the west and the Rio Grande Rift on the east (Fig. 37A). Unlike surrounding areas, which have undergone significant orogenic and extensional deformations since the Paleozoic, the plateau has survived these tectonic events with little internal deformation [Burchfiel *et al*., 1992]. The widespread shallow marine deposition over the Colorado Plateau suggests that this area was below sea level in the Late Cretaceous [Bond, 1976], while the present elevation of the plateau is ~2 km. This change of elevation requires the Plateau to have risen by about 2 km during the time in between.

Both timing and mechanics of Colorado Plateau uplift to its present elevation, however, have remained uncertain. Paleo-botanical studies indicate that the central Rocky Mountains region surrounding the plateau reached their present elevation in the Eocene [Wolfe *et al*., 1998]. Interpretation of basalt vesicularity based on late Cenozoic volcanic rocks along the plateau margins suggests that most of the elevation gain might have occurred in the Miocene [Sahagian *et al.*, 2002]. However, a recent exhumation study based on apatite (U-Th)/He thermochronology pushes the age of Colorado Plateau uplift back to the latest Cretaceous, with a kilometer-scale elevation gain over the southwestern part of the plateau [Flowers *et al.*, 2008; Fig. 34A]. Even though the Plateau is a distinct physiographic unit today [e.g., Spencer, 1996], whether it uplifted as an individual block,

or as part of a broader-scale, synchronous uplift of western United States has been debated [Burchfiel *et al*., 1992; Wolfe *et al*., 1998; Flowers *et al*., 2008].

Various models have been proposed to explain the vertical motion, including crustal thickening [Bird, 1988; McQuarrie and Chase, 2000], removal of mantle lithosphere [England and Houseman, 1988; Spencer, 1996], chemical alteration of the lithosphere [Humphreys *et al*., 2003; Roy *et al*., 2004], and active mantle upwellings [Parsons *et al*., 1994; Moucha *et al*., 2009]. In this chapter, we use mantle convection models to investigate the vertical motion on the plateau associated with Farallon plate subduction.

5.3.2 Subsidence and Uplift of CP due to Farallon Subduction

We calculate the dynamically supported topography due to sub-surface vertical stresses originating from convective flows in the mantle through inverse models. These models, based on the adjoint method, attempted to retrieve past mantle structures by predicting present mantle seismic images through a set of forward and backward calculations (Chapter 3). The adjoint method, with seismic tomography, plate motions, and stratigraphy, has allowed us to better constrain geodynamic processes in the geological past [Liu *et al*., 2008; Spasojevic *et al*., 2009]. By being calibrated with vertical motion proxies beyond the Colorado Plateau (e.g., the WIS formation), the models provide a means to explore the vertical evolution of the plateau since the Late Cretaceous. The resolution of the models (50 km horizontally) is sufficient to predict dynamic topography over the scale of the Colorado Plateau.

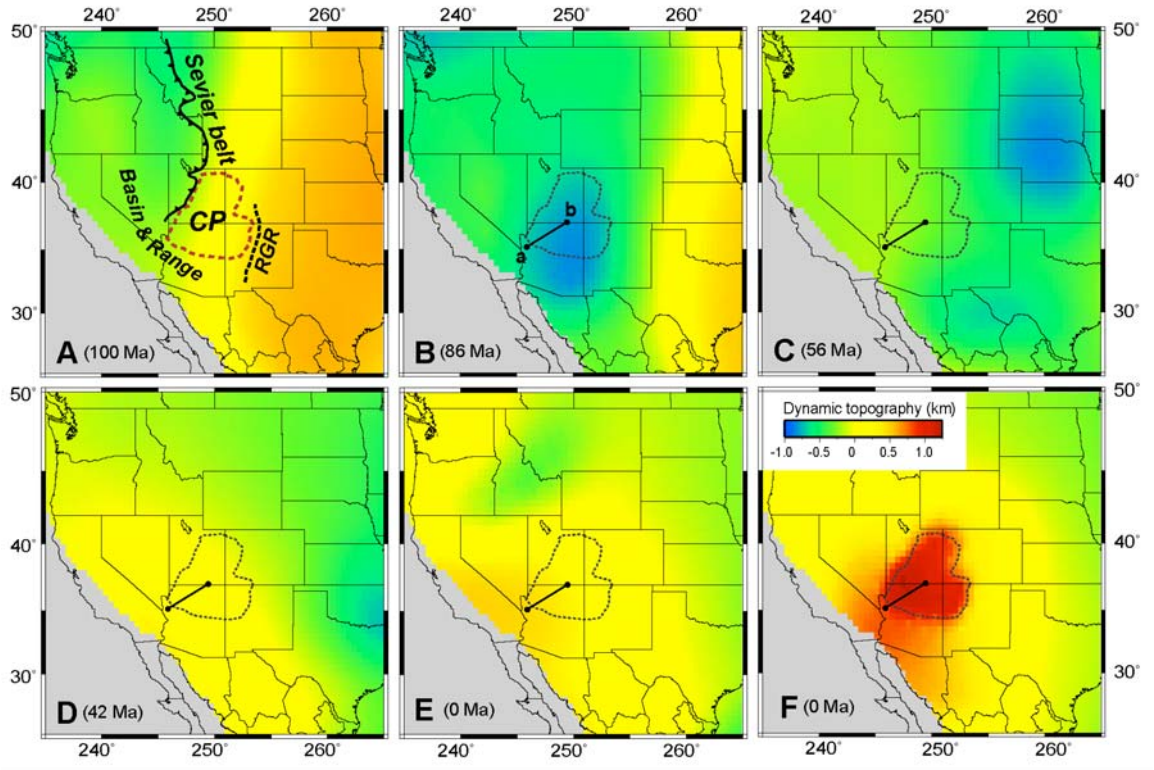

Figure 37 Predicted dynamic topography over the western United States for five different geological times (A–E) based on model M2 (see Table 4), and that for present-day (F) based on M4. Line a-b is the study profile of Flowers *et al*. (2008), same as in Figure 2. Tectonic features (A) are shown for their present-day location (CP - Colorado Plateau; RGR - Rio Grande Rift).

As described in Chapter 4, the inverse dynamic models with three model parameters (upper and lower mantle viscosities and the scaling of seismic variations to temperature associated with the Farallon slab) are constrained by prediction of the Late Cretaceous continental-scale WIS and rates of tectonic subsidence extracted from distributed boreholes [Liu *et al*., 2008; Spasojevic *et al*., 2009]. Our preferred model has only slabs from the Farallon subduction and provides a best fit to both the Western Interior seaway and tectonic subsidence rates (M2 in Table 4). For comparison, we present two

other slab models that fit these constraints less well. One model (M1) has a larger lower mantle viscosity than the preferred model; this model predicted the tectonic subsidence well but had too little marine inundation in the seaway. In another model (M3) we use a larger temperature anomaly and a larger lower mantle viscosity; this model over predicted flooding and its rate of change (through tectonic subsidence rates). Based on parameters from the preferred model for the Farallon slab, we further include the upwelling from the putative buoyant anomaly below the Colorado Plateau (M4).

In order to compare with earlier vertical motion studies, we focus on the southwestern part of the plateau, for which Flowers *et al*. [2008] completed a careful study of exhumation history. The rate of change of dynamic topography from the preferred model, within the Grand Canyon vicinity, is shown in Figure 38A, along with inferences on vertical motion from Flowers *et al*. [2008] and Huntington *et al*. [2010]. The predicted temporal evolution of dynamic topography at several locations along the profile of Flowers *et al*. [2008] is shown in Figure 38B. Map views of dynamic topography over the western United States including the entire Colorado Plateau are shown for five representative times: mid-Cretaceous (100 Ma), Late Cretaceous (86 Ma), Late Paleocene (56 Ma), Middle Eocene (42 Ma), and the present-day (Fig. 37), corresponding to inflexions between subsidence and uplift from the preferred model of dynamic topography (Fig. 38B).

At 100 Ma, before the flat slab stage initiated under the western U.S., the plateau was close to sea level (Figs. 37A and 38). As the Farallon slab moved inland (Fig. 39), the plateau subsided due to the viscous stresses associated with the downgoing slab. The subsidence was sufficiently rapid that by 86 Ma, when the flat slab underplated the

Colorado Plateau (Fig. 39), the entire plateau subsided below sea level with a maximum subsidence at its center (Fig. 37B). As the flat slab migrated to the northeast and sank into the mantle in latest Cretaceous (Figs. 39 and 40), the surface of the plateau began to rebound, causing the first stage of uplift due to the diminishing downward force from the slab (Fig. 37C).

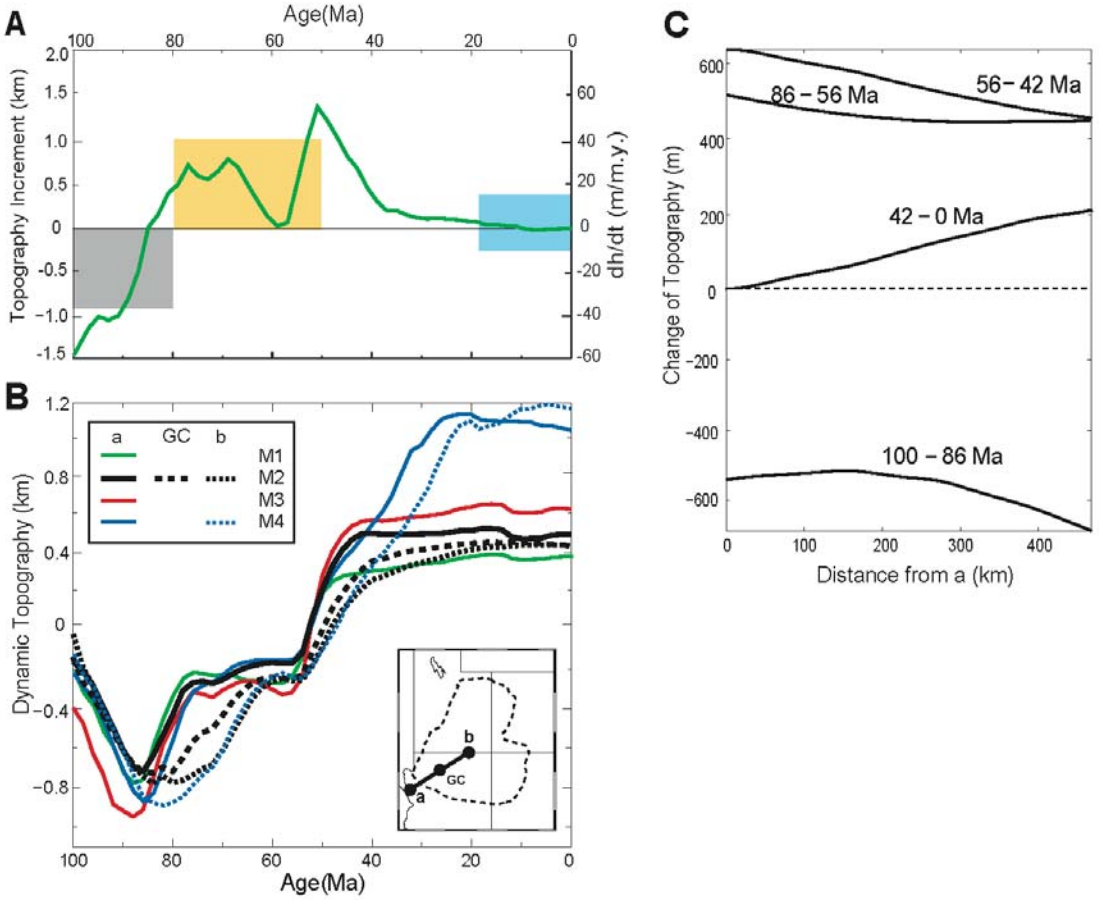

Figure 38 Topographic evolution of the southwest corner of the Colorado Plateau. A: Dynamic subsidence (gray box, isostatically corrected from sediment thickness) and uplift (yellow box) of the southwestern plateau (axis on the left), inferred by Flowers *et al.* [2008]; blue band represents little elevation change inferred by Huntington *et al.* [2010]. Green solid line represents rate of change of

dynamic topography (axis on the right) at the middle of profile (GC - Grand Canyon, in inset map in panel B) from model M2. B: Predicted dynamic topographies since 100 Ma at multiple points along profile (a, GC, and b) based on four different models listed in Table 4. Models M1−M3 show similar trends at all points, so only point a is shown for these models. Addition of positive buoyancy (M4) shows a distinct trend after 40 Ma from other models. C: Changes of dynamic topography during four time intervals along the profile a–b (inset in B) for model M2. These differential topographies illustrate both absolute elevation change and tilting of plateau at different times.

Table 4. Parameters of Models Predicting the CP Dynamic Topography

Model name	η_{UM}	η_{LM}	T_e (◦C)	Active upwelling included?
M1	1.0	30	160	No
M2	1.0	15	160	No
M3	1.0	30	240	No
M4	1.0	15	160	Yes

Note: η_{UM} (η_{LM}) — upper (lower) mantle viscosity, with a reference viscosity 10^{21} Pa s

T_e — effective temperature anomaly

From 56 to 42 Ma, the CP underwent the second stage of uplift (Figs. 37D and 38B) with an instantaneous rate as high as ~60 m/m.y. (Fig. 38A). This fast uplift was caused by removal of the younger part of the Farallon slab from southwest to northeast beneath the plateau, the returning asthenosphere pushing the surface upward (Fig. 40). By 40 Ma, almost the entire slab was removed from beneath the southwest plateau (Fig. 39), and most of the plateau was subject to positive dynamic topography, with the southwest side higher than the northeast (Fig. 37D). From 42 Ma to the present, the southwest margin of the plateau is predicted to have been stable with little vertical motion, while the plateau

interior was uplifted ~200 meters further until the present (Figs. 37E and 38C). The high topography over the plateau since the Eocene in the slab models (M1–M3) was caused by upward return flows generated by the subduction to the north and east of the plateau (Fig. 49).

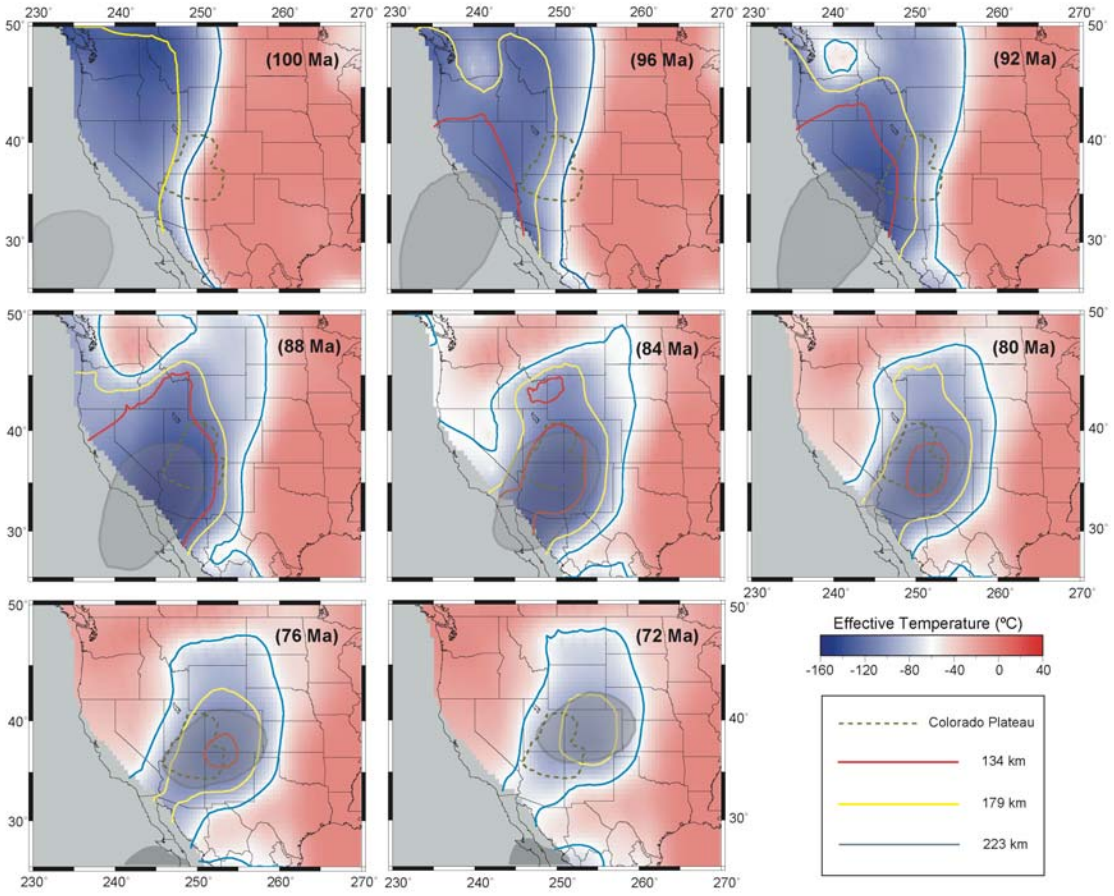

Figure 39 Migration of the Farallon flat slab, surrounding the Shatsky conjugate plateau, with respect to the North American continent during the Late Cretaceous based on the inverse convection model of Liu *et al.* [2008]. The background shows temperature at 220 km depth, while color contours denotes isotherms of temperatures 60 °C lower than the ambient mantle at different depths. The gray area (tracer distribution) indicates the thickest part (core) of the

Shatsky conjugate plateau. A secondary gray area along north Mexico after 76 Ma represents the arrival of the Hess conjugate, causing a secondary flat slab under there.

The predicted subsidence and uplift during Late Cretaceous to Eocene (Fig. 38) correlate well with inferences by Flowers *et al*., [2008]. The southwestern plateau subsided by ~800 m by 85 Ma with an average rate of –40 m/m.y., consistent with the inferred 1.5-km-thick marine deposition (Flowers *et al*., 2008), given an isostatic adjustment factor of ~1.8. Dynamic uplifts occurred quickly following subsidence ca. 85 Ma, with an average rate of 30 m/m.y. until ca. 40 Ma, during which ~1.2 km of elevation was gained, also in agreement with the Flowers *et al*. [2008] results (Fig. 38A). It is worth noting that all models predict that there were two stages of uplift since the Late Cretaceous, with both the trends and timing being consistent with one another, although the magnitude of uplift varies (Fig. 38B).

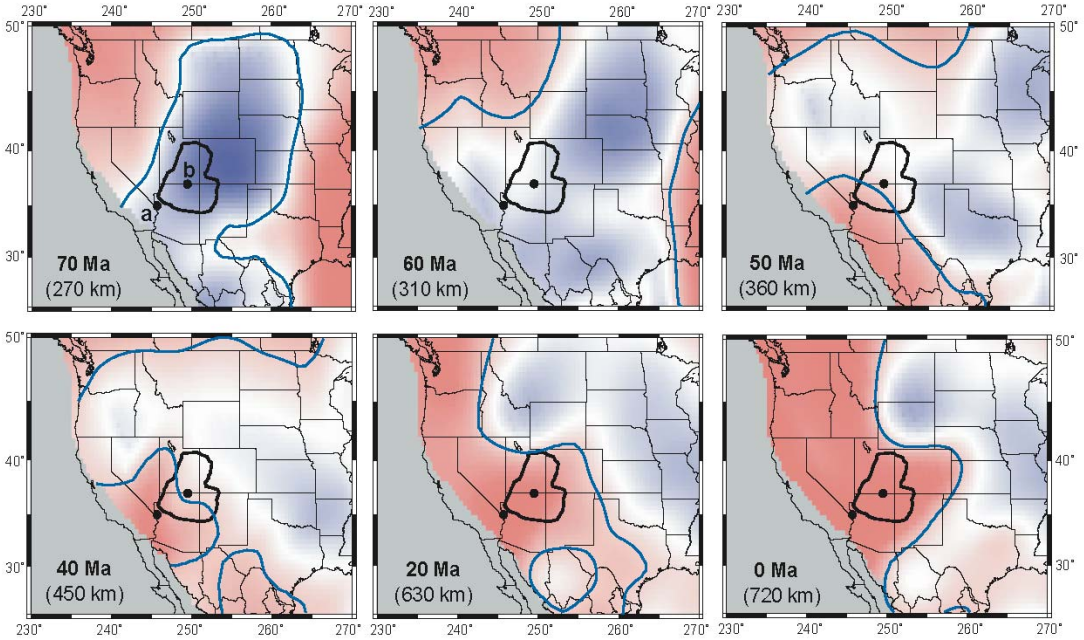

Figure 40 Migration of the Farallon slab inside the mantle beneath the Colorado Plateau after the Late Cretaceous flat subduction from the preferred model in Liu *et al.* [2008]. Each time snapshot corresponds to a different depth where the Farallon slab is best resolved. All time snapshots are projected onto the North American plate. The blue contour represents an isotherm of 30 °C lower than the ambient mantle. Temperature scale is the same as Fig. 35. The two points are the same as in Fig. 33.

5.3.3 Plateau Uplift since Oligocene due to Active Mantle Upwelling

Putative active upwellings associated with upper mantle low seismic velocity anomalies localized beneath the Colorado Plateau were not incorporated in the pure slab models (M1–M3). By including these structures in the inverse model (Fig. 41), the predicted dynamic topography increases by ~700 meters within the Colorado Plateau region (M4) compared to models with only slabs for the present day (Figs. 37E, 37F, and 38B), consistent with recent dynamic models that focus on the late Cenozoic topographic evolution of the plateau [Moucha *et al.*, 2009]. In this case, the earlier evolution of the plateau remains largely the same (Fig. 38B), because the Farallon slab dominates the dynamic topography before the Eocene (Fig. 38B).

We further find that, in models with shallow buoyancy anomalies, lateral variations in lithosphere thickness affect short wavelength surface topographies: A thicker-than-ambient lithosphere associated with the Colorado Plateau predicts the plateau's distinct high topography at present, with sharp topographic gradients on the edge of the plateau (Fig. 37F); a uniform lithosphere thickness leads to a smooth topography with a slightly

reduced magnitude within the plateau relative to that with thicker lithosphere (Fig. 40). The sharp topographic gradient may reflect stress concentration along large viscosity variations inside a convection system, which represents a special mechanism generating surface topographies.

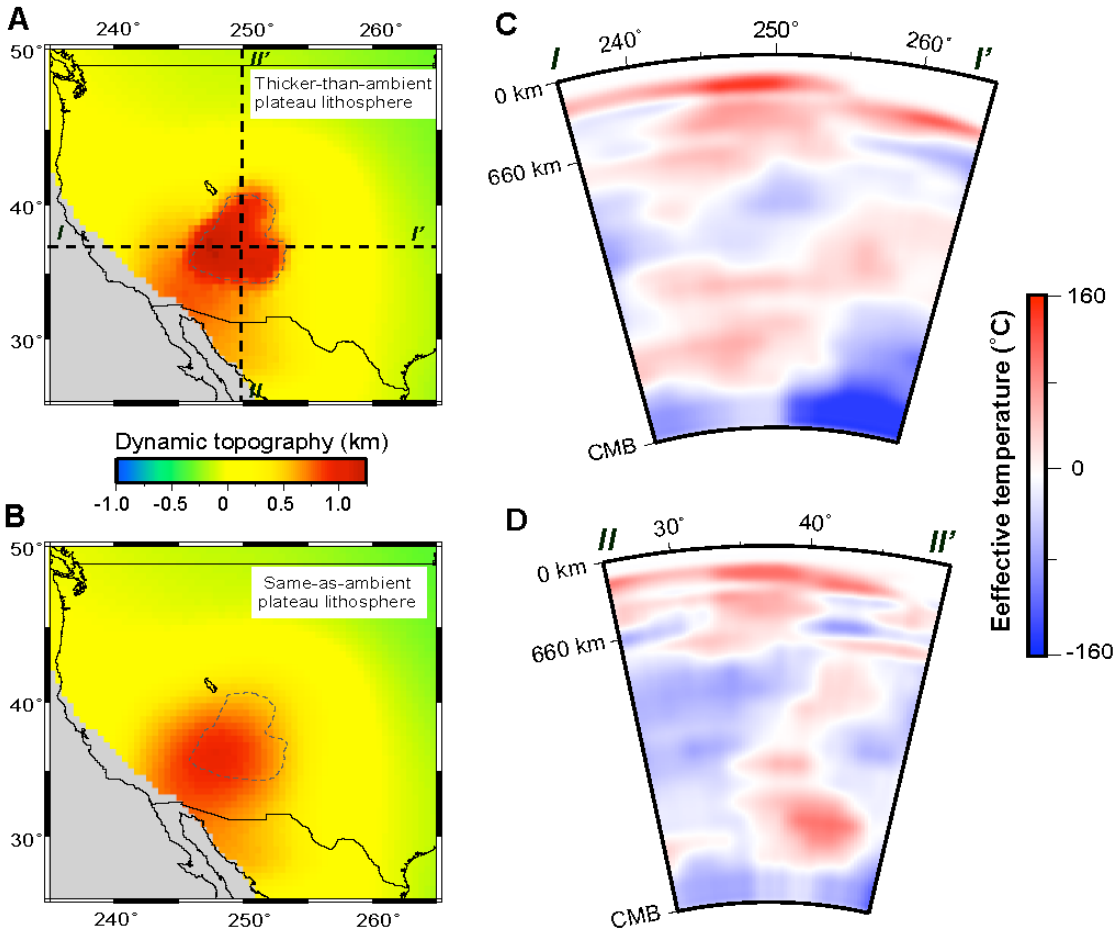

Figure 41 Active upwellings beneath western U.S. and associated surface dynamic topography. A: Predicted present-day dynamic topography by model M4 where the plateau lithosphere is thicker (130 km) than ambient (90 km). The two profiles *I-I'* and *II-II'* indicate cross-sections shown in C and D, respectively. B: Predicted present-day dynamic topography by model M4 where the plateau lithosphere thickness is the same as ambient (90 km). C: East-west vertical profile across the

plateau showing the effective temperature anomaly based on the scaling factor constrained by Liu *et al.* (2008). D: Same as C, but along a north-south vertical profile. In C and D, both the top 150 km signal and that associated with the North American craton are removed.

5.3.4 Tilting of the Plateau during Uplift

Besides the absolute elevation change, dynamic topography also tilts the Colorado Plateau (Figs. 38B and 38C). For example, differential topographies at two end points of a profile (a, b in Figs. 37 and 38) show a tilt in the SW-NE direction.

Specifically, from 100 to 86 Ma, point b subsided more than point a (Fig. 38C), leading to a gentle northeast tilt (Fig. 37B). With the northeastward removal of the flat slab beneath the plateau (Fig. 39), the southwest margin of the plateau rose earlier than the interior (Figs. 38B, C). This northeast tilt became largest ca. 75 Ma, when a differential topography of ~500 meters between the two points was achieved (Fig. 38B).

The tilt diminished at around 60 Ma when the two points (a and b) came to about the same elevation again (Figs. 37C and 38B), driven by the older flat slab moving out to the northeast and younger slab moving below the Colorado Plateau lithosphere from the southwest (Fig. 40). The second uplift phase also accompanied an increase of the northeast tilting, where the southwest margin accumulated >200 m more topography than the plateau interior during the Early Eocene (Fig. 38C), corresponding to the northeast-trending removal of the trailing slab (Fig. 40). Decrease of predicted topography toward the northeast during uplift (Figs. 37 and 38) induced by the northeast-trending subduction of Farallon slab (Fig. 40) may explain the overall northeastward flow direction of the river

drainage systems in central and southern Rocky Mountains [Dickinson *et al*., 1988] and those over the Colorado Plateau [Potochnik, 2001] before the Oligocene.

From 42 to 20 Ma, although absolute uplifts differ among the four models (M1–M4), they all have a diminishing northeast titling, with more topography gained in the plateau interior than the southwest margin (Figs. 38B, 38C). Inclusion of active upwellings (M4) has a change of the tilting direction ca. 15 Ma (Fig. 38B), consistent with the SW carving of the Grand Canyon during the Neogene [Karlstrom *et al*., 2008].

In addition, we note that the predicted dynamic topographies show little change during the Late Cenozoic for all models considered (Figs. 38A, B), consistent with a recent study of clumped carbon isotopes from lacustrine deposits showing that the Colorado Plateau underwent little vertical motion since around 20 Ma (Fig. 38A) [Huntington *et al*., 2010].

5.3.5 Discussion

With an inverse model that satisfies a range of observational constraints, we predict the evolving dynamic topography over the Colorado Plateau from 100 Ma to the present. The area in southwest Utah and northwest Arizona started to raise ca. 85 Ma (Fig. 38B), which seems to mark the inception of the Laramide uplift, while ensuing uplifts until Late Eocene coincide with the entire Laramide orogenic events [DeCelles, 2004]. The predicted two-phase uplift prior to Oligocene seems to agree with the stratigraphically inferred two-stage Laramide orogeny in the southern Rocky Mountain area with an intervening Early

Paleocene deformation hiatus [Cather and Chapin, 1990], although we still do not understand the exact relationship.

In Section 5.2, we show that the flat slab inside the Farallon plate represents a subducting oceanic plateau whose extra initial buoyancy caused the flattening. This also poses another question about the inverse dynamic model: When exactly did the oceanic plateau lose its buoyancy? In other words, will the predicted dynamic subsidence over the western U.S. (Fig. 37) change upon considering this additional complexity during subduction? If the thick crust of the oceanic plateau had completely eclogitized by ~86 Ma, meaning the plateau density did not differ from the ambient lithosphere, the predicted pattern of subsidence is Fig. 37 will hold true.

However, if the eclogite phase transformation was not complete by this time and the plateau still buoyant, the induced surface subsidence above the plateau will be smaller than outside, given the same flat slab geometry from inside out of the plateau area. Because the predicted subsidence over the Colorado Plateau agrees with inferred rock uplift [Flowers *et al*., 2008], we would expect the region right above the flat slab but beyond the thick oceanic plateau, say in Wyoming, to experience more dynamic subsidence than shown in Figure 37. In fact, the Cretaceous sediment isopach does show thicker marine deposits over Wyoming than areas to the south [DeCelles, 2004], and similarly backstripped residual subsidence also decreases southward from Wyoming [Pang & Nummedal, 1995]. Another useful constraint comes from the geoid: Right above the currently subducting Inca plateau in Peru, there is a local geoid minimum [Fig. 42]; this pattern does not correlate well with the surface topography but does with the seismic

image, which suggests deeper mass deficit and indicates that the Inca plateau may have not lost all its extra buoyancy yet.

As a result, this suggests that our inverse dynamic model may have underestimated the density of the Farallon slab beyond the oceanic plateau. Consequently, the lower mantle viscosities inferred by predicting the WIS and borehole subsidence curves is also likely underestimated, since it trades off with slab density (Chapters 3, 4). Of course, further refinement of these mantle properties has to be subject to future research.

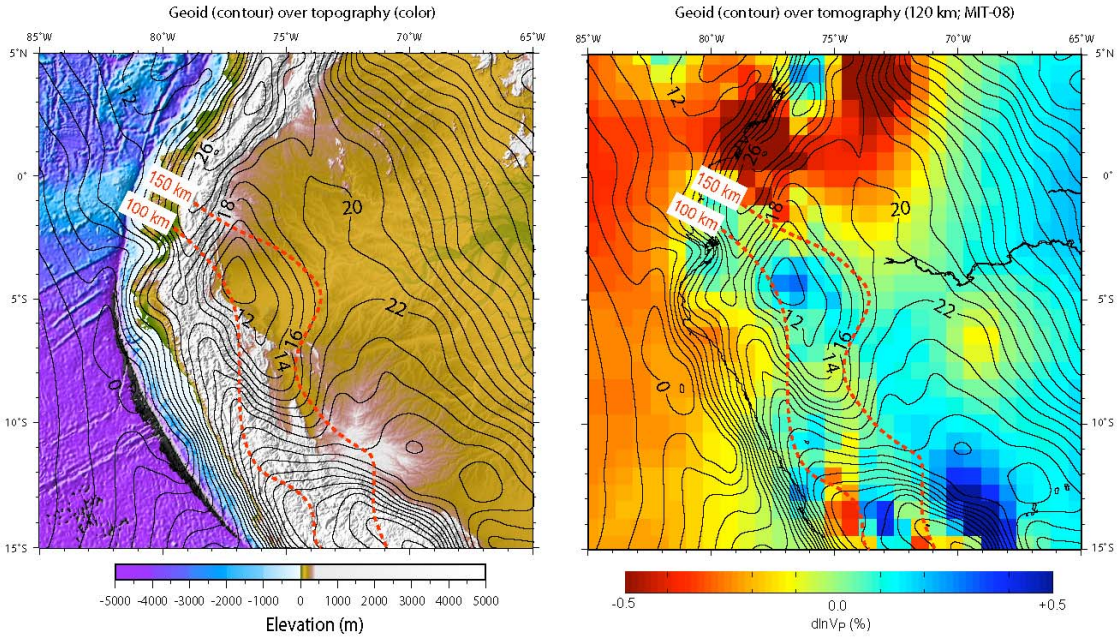

Figure 42 Same as Figure 33, only that both topography (left) and seismic tomography (right) are overlain by geoid (black contours incrementing by 8 meters per interval). Note the geoid low right above the flat slab according to the Inca plateau, indicating that the plateau is still buoyant at this stage of subduction.

When the Colorado Plateau rose above the surrounding areas and formed a unique topographic unit remains unknown. The inverse convection models suggest that Colorado Plateau uplifted high above sea level by the end of Eocene, as part of a broader uplift of the western United States (Fig. 37D), consistent with the high elevations inferred from fossil botanical records for areas surrounding the plateau and the adjacent Basin and Range province [Wolfe *et al.*, 1998]. During the Oligocene, buoyant upwellings further raised the plateau locally (Figs. 38B and 41), while a thicker-than-ambient lithosphere caused sharp edges to the plateau topography, due to enhanced coupling to the upper mantle (Fig. 37F). This suggests that the Colorado Plateau could have became a more isolated crustal block following lithospheric thinning associated with Basin and Range extension. High topography in the Rocky Mountains is not explained by our proposed mantle forces (Fig. 37), which could have resulted from crustal shortening during the Farallon flat subduction [Bird, 1988].

Because the adjoint models satisfy multiple observational constraints during the Late Cretaceous to Early Tertiary, including both the WIS stratigraphy (Chapter 4) and inferences from thermochronology (Chapter 5), we think the predicted vertical evolution of Colorado Plateau before the Late Eocene is likely to be robust. The uplift history after this time associated with the occurrence of active upwellings, however, is less well constrained, where the prediction is only validated by a recent study of clumped carbon isotopes since the Miocene [Huntington *et al.*, 2010]. Given the fact that the nature of low velocity anomalies beneath the CP is less well understood than the Farallon slabs, and that considerable discrepancies in both the magnitude and pattern of these low seismic velocity

anomalies still exist [Grand, 2002; Wang *et al.*, 2007; Burdick *et al.*, 2008; Tian *et al.*, 2009], we propose the dynamic evolution of the putative active mantle upwelling beneath the Plateau may still need more comprehensive constraints, especially in identifying their composition as being chemical (e.g., containing water), thermal or phase changes (e.g., partial melt). As a result, some other mechanisms proposed earlier could still contribute to the Plateau uplift to some extent. For example, the conceptual model of chemical alteration of the Plateau lithosphere during the Farallon flat subduction [Humphreys *et al.*, 2003] argues for uplift due to compositional changes within the lithosphere. On the other hand, a thermal-mechanical model of lithosphere heating due to thermal diffusion after the flat subduction terminates [Roy *et al.*, 2009] provides a mechanism for the topographically higher Plateau rim than the interior.

In summary, the predicted uplift of ~1.2 km for the Colorado Plateau from Late Cretaceous to Eocene was induced by northeastward translation of the Farallon slab, which was augmented by ~700 meters during Oligocene in response to active mantle upwellings beneath the plateau [Fig. 38B]; combined, the two processes largely raised the Colorado Plateau to its current elevation. Because the inverse models are constrained by various geological data from the Late Cretaceous to the present, our predicted trends and timing of plateau vertical evolution could represent important components of the actual motion.

5.4 Implications for the Evolution of the Western Interior Basins

5.4.1 Migrating Depocenter within the WIS Subsidence

Upper Cretaceous strata of the United States western interior basin (WIB) are well suited for quantitative subsidence studies because of precise stratigraphic knowledge [Dyman *et al.*, 1994]. A recent backstripping study along two sections inside the western interior basins were performed by Liu *et al.*, [in revision]. One section extends across central Utah and Colorado (UT–CO); the other across southern Wyoming (WY). Decompaction and flexural backstripping of the UT–CO stratigraphic section are conducted by procedures described in Liu & Nummedal [2004]. The difference between the total decompacted subsidence and the amount of subsidence caused by flexural loading of the Sevier thrust belt, and sediments and water within the WIB, i.e., the "residual" subsidence, across both sections, demonstrates the presence of a dominant, long-wavelength component at all times (Figs. 43 and 44).

As shown in Figs. 43 and 44, a long wavelength (~1000 km) residual subsidence migrated from west to east along both sections. The magnitude of subsidence, averaged along the whole sections, follows a pattern of an initial increase to a maximum in "mid-life" of basin evolution, and a subsequent decrease. A trend of landward translation of the whole long-wavelength subsidence profile in both sections is observed. This trend is characterized by maximum subsidence in the west during time intervals 1 and 2 (Figs. 43, 44), transforming into an eastward-moving trough-shaped subsidence profile during intervals 3 and 4.

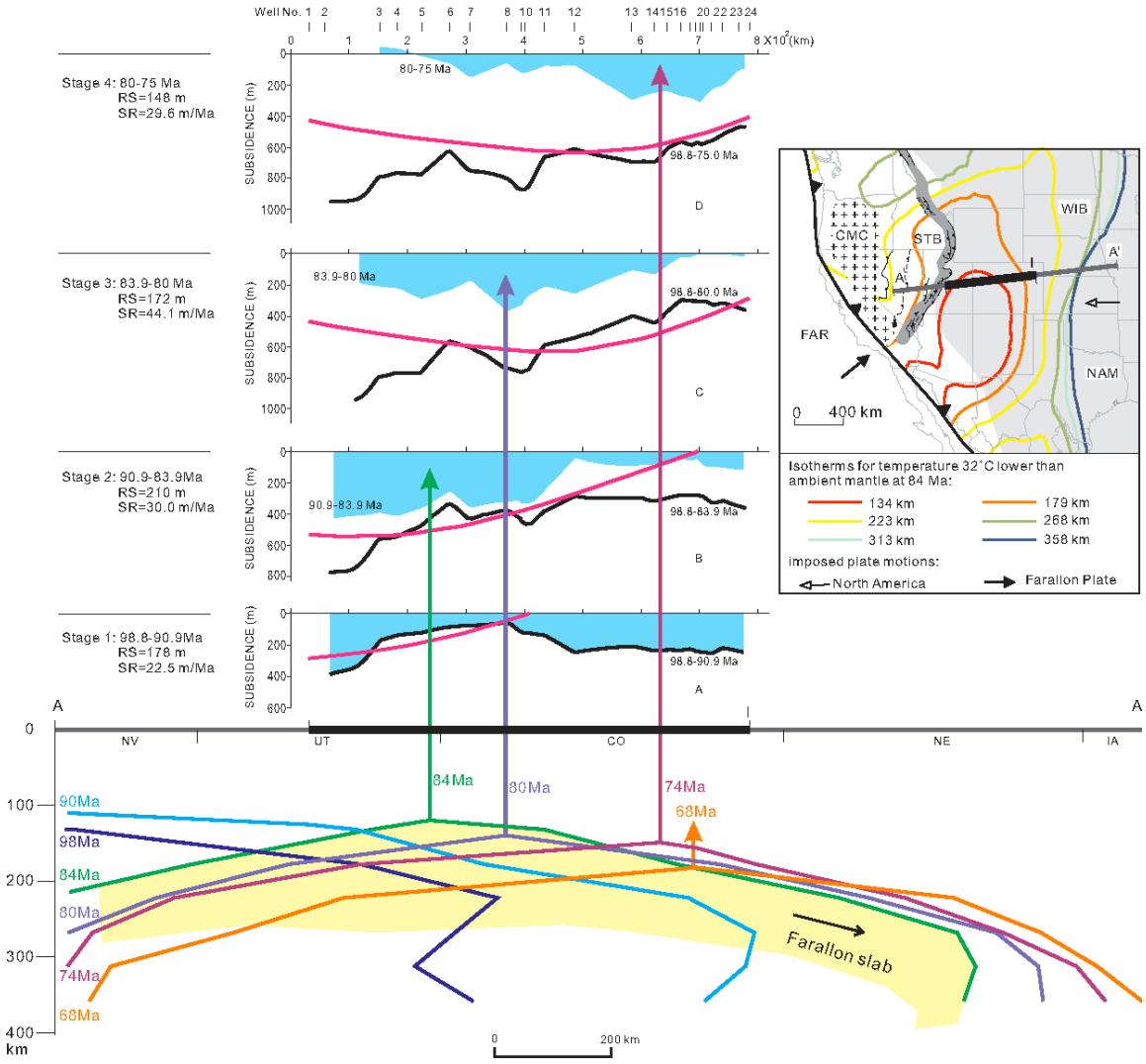

Figure 43 (Upper) Profiles of backstripped residual subsidence and their comparison with modeled dynamic subsidence across UT-CO over four time intervals. Location of this section is shown with the heavy dark line A-A' in the inset map. Black curves and blue-colored bands represent cumulative and incremental residual subsidence, respectively, and the pink curves represent modeled cumulative dynamic subsidence, for each time intervals. RS: incremental residual subsidence averaged over the whole profile; SR: averaged incremental subsidence rate. (Lower) Cross-sectional view of the flat Farallon plate from 98 to 68 Ma, along Section C-C' (heavy gray line in the inset map). Color lines indicate the upper boundary of the slab at different times, represented by an isotherm 32˚C lower than ambient mantle. The whole cross-section of flat slab at 84 Ma is highlighted in light yellow with black arrow indicating its moving direction. Vertical

arrow-lines indicate locations of the slab crests. The inset map shows main tectonic elements (the Cordilleran Magmatic Arc (CMC), Sevier thrust belt (STB), Western Interior Basin (WIB), Northern America (NAM), and Farallon plate (FAR)), and the depth to the upper boundary of the reconstructed Farallon slab at 84 Ma (colored contours). The North American plate is plotted in its present-day coordinates.

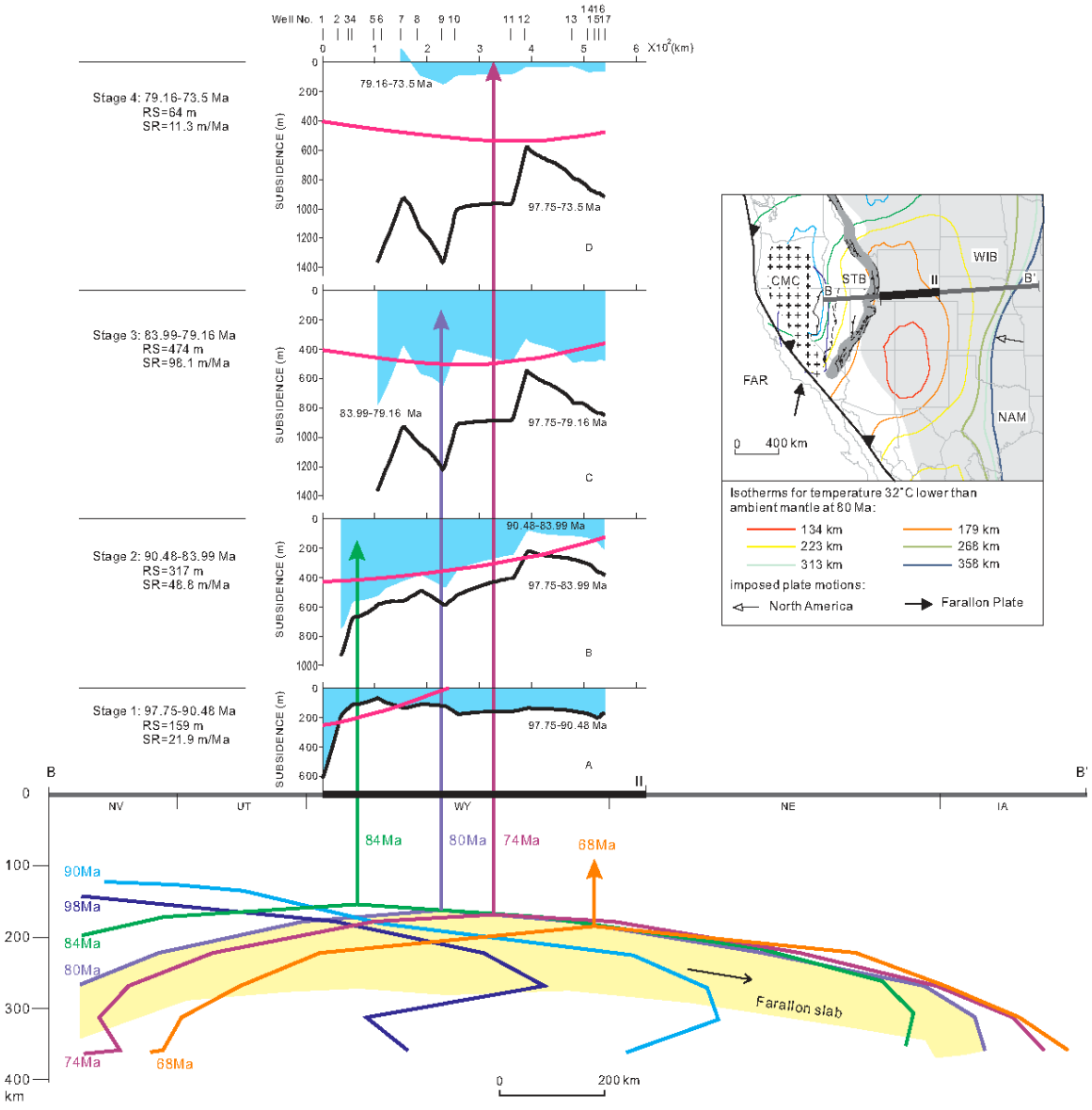

Figure 42 Same as Figure 41, only that this is for the WY section.

This temporal evolution of subsidence suggests that the subducting Farallon plate caused a regionally focused surface subsidence that moved inland over the North American plate. Convection models assuming subduction with a fixed geometry of down-going slabs relative to the overriding plate do not fit this observation, because in such cases, the induced dynamic subsidence patterns on the overriding plate are also stationary. Models involving gradually shallowing and/or steepening subducting oceanic slabs have been proposed to explain the migration of volcanism over the western United States [Coney and Renolds, 1977] and the continental scale tilting of North America [Mitrovica *et al*., 1989]. These earlier models suggest an overall broadening (narrowing) in the extent of dynamic subsidence as the slab shallows (steepens), but not the successive landward shift of subsidence centers, as revealed by our backstripped results.

5.4.2 Implication for Oceanic Plateau Subduction

The observed evolving long-wavelength residual subsidence seems to be consistent with our inverse convection models. By comparing the accumulative residual subsidence with predicted dynamic topography from the inverse model, we find that the overall eastward migration matches both sections (Figs. 43, 44), and magnitudes are also consistent along the UT-CO section (Fig. 43). We, therefore, conclude that these long-wavelength residual subsidence represent the dynamic subsidence caused by the passage of the flat Farallon slab.

Specifically, the eastward-dipping limb of the flat slab before 90 Ma causes the widespread small magnitude subsidence, whereas the high rate of subsidence to the west is

due to the shallower western edge of the slab (Figs. 43, 44, stage 1). As the slab translates inland with its crest beneath eastern UT (Fig. 43) and western WY (Fig. 44) at ~84 Ma, the dynamic subsidence shifts eastward with its highest rates occurring right above the center of the flat slab (Figs 43, 44, stage 2). The increase in dynamic subsidence from stage 1 to 2 is due to the eastward motion of the slab that broadens the subsidence area, and the shallowing of the slab beneath the continent. At ~80 Ma, the dynamic subsidence center moves to western Colorado (and the middle of Wyoming) and the averaged subsidence further increases (Figs 43, 44, stage 3), consistent with it being induced by the shallow flat slab that causes the whole surface profile to subside. The symmetric geometry of the flat slab defines the trough-shaped subsidence profiles. After 80 Ma the Farallon plate changes its direction with respect to North America from east to northeastward during which the Farallon slab sinks deeper into the mantle. Because the bulk of the flat slab was to the south of Wyoming during most of the Late Cretaceous (inset map of Figs 43, 44), the UT-CO section experiences its continued effects, but Wyoming is north of its zone of impact. This generates the continued high subsidence rates in eastern Colorado (Denver basin) to the end of the Cretaceous, whereas dynamic subsidence in Wyoming at this time essentially comes to an end. The migration of subsidence profiles and their correlation with the inferred Farallon slab, therefore, reveals that the western United States underwent dynamic subsidence subject to buoyancy-induced mantle flow, similar to what Australia may have experienced during the Cretaceous [Gurnis *et al*., 1998].

The different rates of dynamic subsidence inferred from the two profiles, with WY experiencing a faster subsidence than UT-CO during time intervals 2 and 3 (Figs. 43, 44),

are not explained by our convection model. Accordingly, the flat slab under WY is deeper than that under UT-CO, and the slab thickness, thus negative buoyancy, under WY is also smaller. If the slab had the same composition under the two profiles, both of these factors suggest a smaller dynamic subsidence along the WY section, opposite of what is observed. Whereas the overall geometry of the localized flat slab is constrained by seismic tomography, its regional variation in composition is not known. This high-resolution stratigraphic data provide additional constraints on the dynamic property of the inferred flat slab: the observed larger dynamic subsidence in WY than in UT-CO strongly argues for a lower density associated with the thickened flat slab.

An ideal candidate for causing such a flat slab is a subducting oceanic plateau, a conclusion reached independently (Chapter 5.2). In this case, the extra buoyancy associated with the thick oceanic crust of the plateau would cause less dynamic subsidence than the denser slab underlying the Wyoming lithosphere to the north. Our argument that the Shatsky conjugate plateau subducted beneath North America during the Late Cretaceous is further supported by this new stratigraphic data. On the other hand, future models simulating the oceanic plateau subduction beneath the western U.S. should attempt to address the problem raised in Figure 45, where the maximum dynamic subsidence occurred to the north of the thick slab, rather than right above (Fig. 45b). Therefore, surface rebound (i.e., uplift) accompanying removal of the oceanic plateau (Fig. 45c) is also likely to have affected areas to the north of Colorado and Utah more than our inverse model have predicted (Figs. 33, 34).

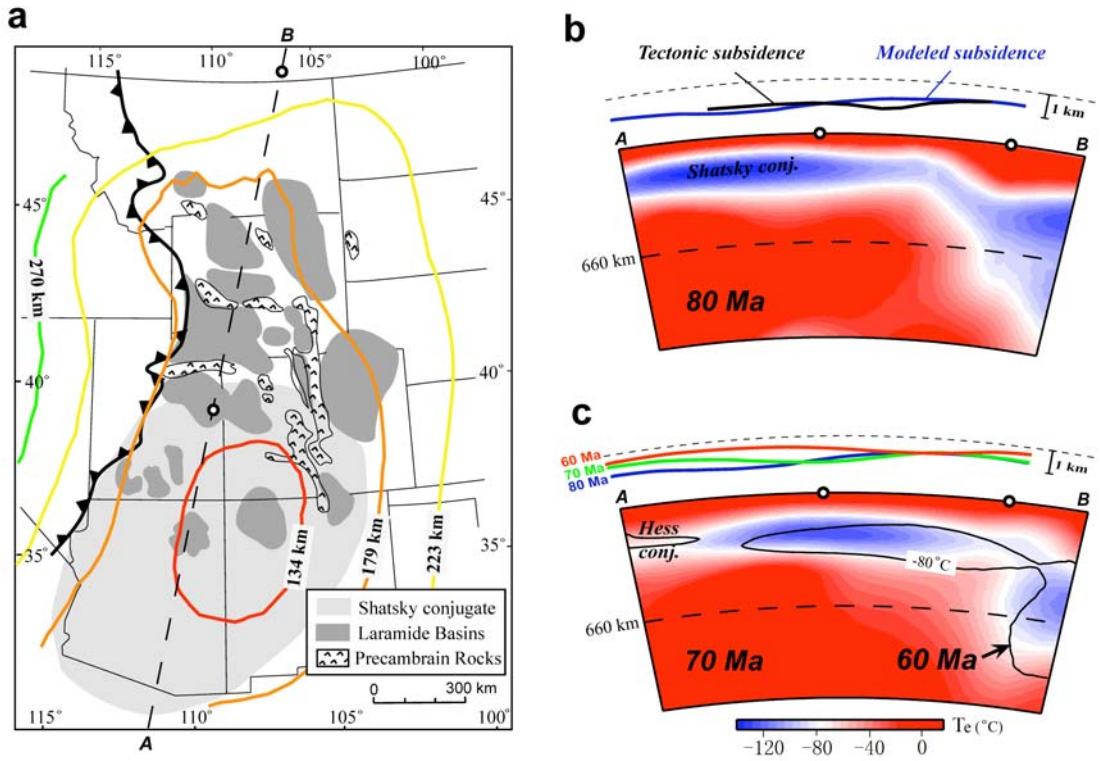

Figure 45 New constraints for improving the inverse model. a) Map view of major Laramide mountains and basins, overlain by slab contours (color) from the inverse model. Profile A−B marks the location of cross-sections shown in b & c. b) Recovered slab geometry from tomography, and predicted dynamic topography that is phased shifted southward relative to observed tectonic subsidence. c) Regional surface uplift accompanying removal of the flat slab from underneath. Color shows the 70 Ma slab geometry, while black contour is for an isotherm (80 °C lower than ambient) at 60 Ma. Predicted Shatsky (80 Ma) and Hess (60 Ma) conjugate plateaus are also shown.

The discrepancy between predicted dynamic topography and observed residual subsidence indicate the inadequacy of the inverse model, and therefore, also provides new constraints on further improving the inverse dynamic model, especially in simulating the exact process of oceanic plateau subduction. First of all, the difference between profile UT-

CO and WY suggests the oceanic plateau maintains at least part of its initial buoyancy at ~80 Ma, consistent with the observation on the present-day Inca plateau, which correlates with a geoid low (Fig. 42). This requires future models to incorporate the appropriate basalt-eclogite phase transformation to accommodate this process of density change.

Second, although patterns of the cumulative subsidence along the UT-CO profile are well predicted, predictions of their time derivatives (differential subsidence, Figs. 43, 44) are not satisfactory. This shows up as a gradual overprediction of dynamic subsidence toward the end of the study period (Fig. 43, 44, stage 3, 4). We also encountered this problem when attempting to predict tectonic subsidence rates from borehole, where a systematic increase of subsidence rate toward the east is predicted, which was absent in the data (Section 4.3). While considering the chemical buoyancy of the oceanic plateau may improve the fit, this may also require the existence of a low viscosity mantle wedge that diminishes surface subsidence above [Billen and Gurnis, 2003].

5. 5 Subsidence of the U.S. east coast since the Eocene

North America has been suggested as a dynamic topography low by using either density structures inferred from seismic tomography [Hager *et al*. 1985; Steinberger, 2007] or the history of subduction [Lithgow-Bertelloni and Richards, 1998]. Both global [Grand, 2002; Ritsema and van Heijst, 2000; Li *et al*., 2008] and regional [Ren *et al*., 2007] seismic tomography models show a linear high seismic velocity anomaly beneath eastern North America at mid-mantle depths, interpreted as the remnants of Farallon plate subduction [Bunge and Grand, 2000; Ren *et al*., 2007]. Independent of these geophysical concepts, Miller *et al.* [2005] made new sea-level estimates that putatively reflect eustasy, based on the backstripping of sedimentary sections at five boreholes located on the New Jersey coastal plain [Van Sickel *et al*., 2004]. The maximum long-term sea-level change is around 70 m [Miller *et al*., 2005], which is lower than most other published global sea-level estimates (Fig. 46A).

Comparison between the Miller *et al*. [2005] long-term sea-level estimate with other estimates shows that there appears to be a significant discrepancy between maximum Late Cretaceous sea levels on the order of 50–200 meters (Fig. 46). Consequently, we hypothesize that the estimate of Miller *et al*. [2005] reflects regional, rather than global sea-level variations on the 10^7-year scale considered in global dynamic models. Further, we suggest that the discrepancy is driven by a dynamic subsidence of the eastern areas of the United States but the magnitude of the subsidence has been somewhat smaller than the fall in global sea level over the same period.

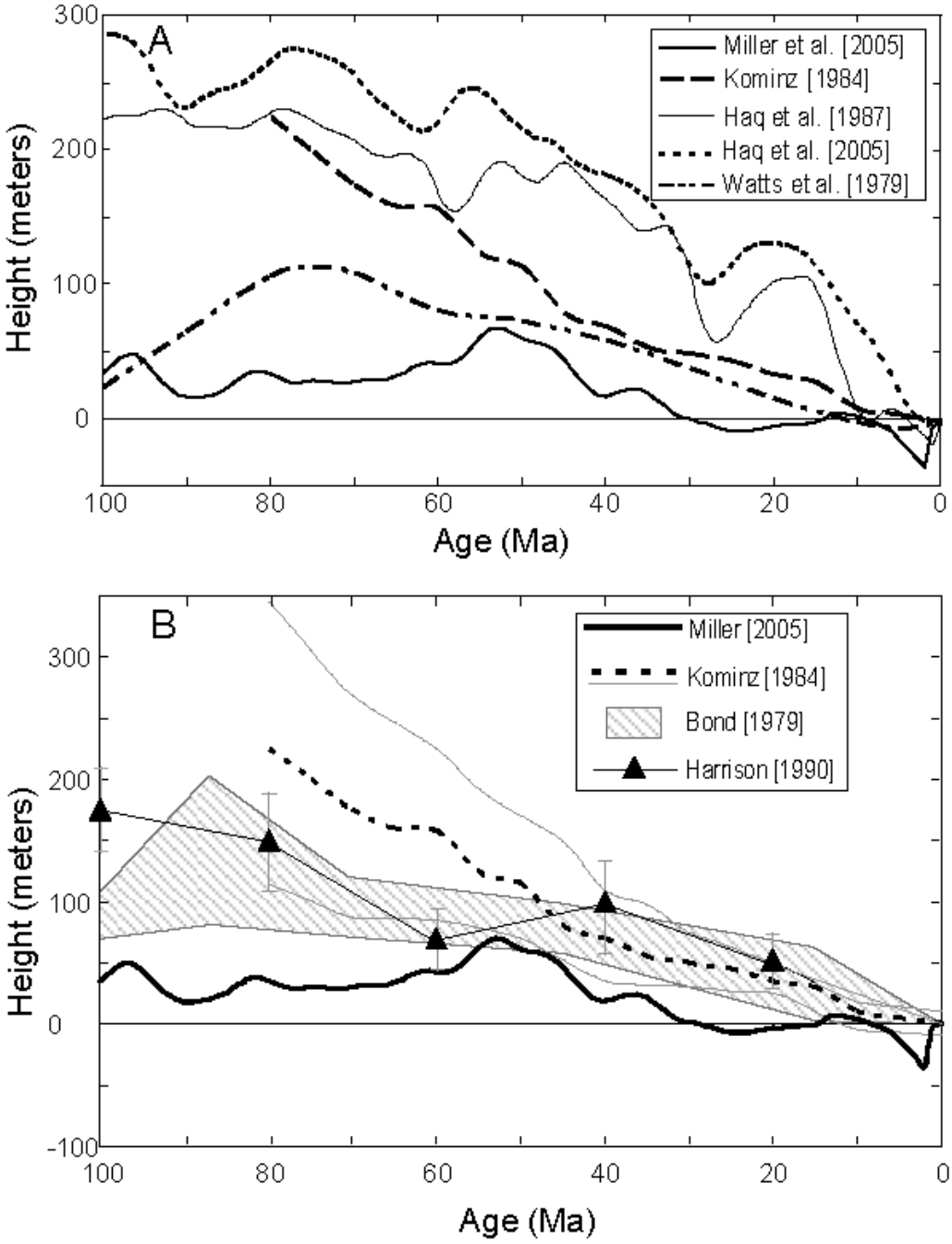

Figure 46 [from Spasojevic *et al*., 2008] Comparison between sea-level curves. (A) Comparison between Haq *et al.*, [1987], Haq and Al-Qahtani [2005], Kominz [1984], and Watts and Steckler [1979] curves with sea-level curve derived for New Jersey coastal plain [Miller *et al.*, 2005] for last 100 million years, smoothed by a 10 m.y. cosine arch filter to isolate long-term sea-level change. (B) Comparison between sea-level estimates based on the analysis of continental flooding

[Harrison, 1990; Bond, 1979] and Miller *et al.* [2005] and Kominz [1984] sea-level curves. Thin continuous lines indicate maximum and minimum estimates from Kominz [1984], hatched area range of estimates from Bond [1979], and black line with triangles average estimates of Harrison [1990] with associated error bars.

Both migration of paleo shorelines in the eastern United States [Spasojevic *et al.*, 2008] and adjoint models of mantle convection (Chapter 4) are used to determine the requisite dynamic subsidence at the east coast. Although the paleo shorelines analysis is characterized by relatively large uncertainty, the trends from the paleo shorelines indicate at least 50 m, and possibly as much as 200 m of subsidence since the Eocene. Details of the paleo shorelines analysis can be found in Spasojevic *et al.* [2008].

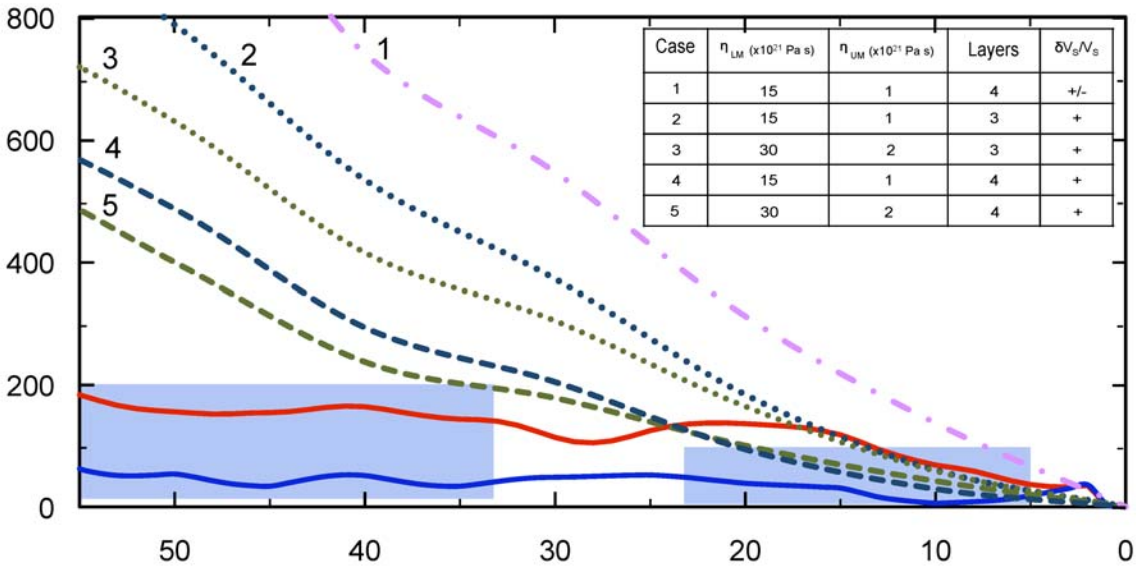

Figure 47 Predictions of the U.S. east coast subsidence. Dynamic topography change for a well in New Jersey coastal plain (coordinates 285°30', 39°30'N) from five dynamic models is shown with colored dotted and dashed lines, solid red and blue lines show difference between sea-level models of Haq and Al-Qahtani [2005] and Miller *et al.* [2005], and Kominz [1984] and Miller *et al.* [2005], respectively. Blue colored boxes show estimated subsidence range from paleo shoreline analysis [Spasojevic *et al.*, 2008] for Eocene and Miocene. Table insert shows model

parameters (η=viscosity, LM=lower mantle, UM=upper mantle viscosity, $\delta V_S/V_S$= seismic anomaly with positive (+) or both positive and negative (+/-) signals included).

All inverse models that we explored predict Tertiary subsidence of the U.S. east coast (Fig. 46). Models that yielded the best fits to WIS borehole subsidence (Fig. 47, cases 2–3) predict 700–900 m subsidence since the early Eocene, and 250 m since the early Miocene. Models scaling both positive and negative S wave anomalies (Fig 47, case 1) yield the largest estimate of post Eocene subsidence. These models (Fig. 47, cases 1–3) overestimate the amount of subsidence, compared with paleo-shorelines and sea-level discrepancies. In order to reduce dynamic subsidence since 55 Ma, we introduce an additional viscosity layer in the uppermost mantle that was not required to fit Late Cretaceous flooding and subsidence. This layer extends from the base of the lithosphere to 410 km depth with a viscosity of 10^{20} Pa s, while the transition zone has a viscosity of 10^{21} Pa s. Estimates of dynamic subsidence since the early Eocene for this four-layer mantle are 480–560 m (Fig. 47, cases 4–5), consistent with subsidence estimates based on paleo shorelines and sea-level discrepancies. Models with additional layer in the upper mantle yield the same Late Cretaceous subsidence and flooding as the three-layer models, given that lower mantle viscosity is the same in both three- and four-layer model, and that upper mantle viscosity in 3-layer model is the same as transition zone viscosity in the four-layer model.

Therefore, the proposed dynamic subsidence can possibly explain the discrepancy between the Miller *et al.* [2005] sea-level curve and other eustatic curves [Spasojevic *et al.,* 2008].